Research Square

Preprints are preliminary reports that have not undergone peer review.
They should not be considered conclusive, used to inform clinical practice,
or referenced by the media as validated information.

A Low-Processing Graphite–Paraffin Biocomposite with Torrefied Cagaita Biomass for Enhanced Charge Storage

Eric M. Garcia

eric@ufsj.edu.br

Federal University of São João del-Rei

Hosane A. Taroco

Federal University of São João del-Rei

Julio O.F Melo

Federal University of São João del-Rei

Ana P. C Madeira

Federal University of São João del-Rei

Research Article

Keywords:

Posted Date: November 2nd, 2026

DOI: https://doi.org/10.21203/rs.3.rs-11341664/v1

License: This work is licensed under a Creative Commons Attribution 4.0 International License.
Read Full License

Additional Declarations: No competing interests reported.

A Low-Processing Graphite–Paraffin Biocomposite with Torrefied Cagaita Biomass for Enhanced Charge Storage

Eric M. Garcia, Hosane A. Taroco, Julio O.F Melo and Ana P. C Madeira

DECEB - Department of Exact and Biological Sciences - Federal University of São João del-Rei (UFSJ) City : Sete lagoas. State : Minas Gerais. Country : Brazil.

Keywords: Torrefied biomass; Cagaita pulp; Graphite–paraffin biocomposite; Sustainable composites; Charge storage; Interfacial relaxation

Corresponded author e-mail : eric@ufsj.edu.br

Abstract

A sustainable graphite–paraffin biocomposite was developed by directly incorporating torrefied cagaita (*Eugenia dysenterica* DC) pulp biomass (TBCP) into the composite matrix. The biomass was mildly treated at 250 °C for 1 h in air, without chemical activation or inert-atmosphere carbonization. Electrodes containing 0–15 wt.% TBCP were evaluated in 1.0 mol L^{-1} NaOH, with the highest response obtained at 5 wt.% TBCP (≈13 mF cm^{-2}), indicating an optimum balance between the biomass-derived contribution and preservation of the conductive graphite network. Trasatti analysis showed that TBCP increased the total accessible capacitance from 0.219 to 25.68 mF cm^{-2} and the apparent electrochemical porosity from 18.6 to 91.4%. Chronoamperometric analysis further showed an increase in total apparent areal capacitance from 0.113 to 19.37 mF cm^{-2}, while the characteristic time of the dominant slow relaxation process decreased from 3.958 to 1.744 s. Galvanostatic measurements yielded 21.05 mF cm^{-2} at 1.0×10^{-4} A. These results demonstrate that a small amount of minimally processed lignocellulosic biomass can effectively enhance charge storage in graphite-based composites, providing a simple and sustainable route to improved electrochemical performance.

Keywords: torrefied biomass; cagaita pulp; graphite–paraffin electrode; charge storage; interfacial relaxation.

1. Introduction

Graphite–paraffin composites are simple, low-cost, and versatile electrochemical platforms whose properties can be tailored through the incorporation of functional materials into the bulk matrix. In these composite architectures, graphite provides the main conductive framework, while paraffin acts as a binder that ensures mechanical cohesion and allows surface renewal by simple polishing. Although graphite–paraffin electrodes have been predominantly explored for electroanalytical and sensing applications, modification of their carbonaceous matrix may also alter fundamental interfacial properties, including the electrochemically accessible surface area and charge-storage behavior [1,2]. In this context, biomass-derived materials are attractive modifiers because of their renewable origin and chemically heterogeneous surfaces containing a variety of oxygen-containing functional groups.

Biomass-derived carbons with high capacitive performance have been widely reported; however, such performance is often achieved through relatively complex processing routes. For example, lignocellulosic biomass has been subjected to dissolution, gelation, freeze-drying, carbonization, and subsequent KOH activation to obtain hierarchical porous carbons for supercapacitor applications [3]. These materials are then commonly combined with conductive additives and polymeric binders, such as PVDF, and deposited onto metallic substrates [3]. Although these strategies are effective for maximizing charge storage, the multiple processing steps increase fabrication complexity. An alternative approach is therefore to investigate whether a mildly processed biomass can be directly incorporated into a simple graphite–paraffin matrix to

improve electrochemical accessibility while preserving the structural and conductivity advantages of the graphite network.

The interfacial capacitance of graphite is highly dependent on surface structure and chemistry. A commercial graphite rod electrode, for example, exhibited a double-layer capacitance of approximately 5.8 μF cm^{-2} in 0.5 M Na_2SO_4 [4]. Highly oriented pyrolytic graphite (HOPG) also exhibits a relatively low interfacial capacitance when the basal plane is exposed. In 1 M NaOH, a minimum space-charge capacitance of approximately 2.5 μF cm^{-2} was reported for a fresh HOPG basal plane, whereas surface damage induced by hydrogen evolution and the resulting increase in edge-plane content produced an approximately one-order-of-magnitude increase in capacitance [5]. Other studies have likewise demonstrated pronounced differences between basal- and edge-oriented graphite surfaces, with the latter exhibiting much higher capacitance because of the contribution of electrochemically active oxygen-containing functionalities, including quinone/hydroquinone redox groups [6,7]. These observations demonstrate that relatively small changes in interfacial chemistry and surface accessibility can strongly influence the charge-storage response of graphite-based electrodes.

From this perspective, lignocellulosic biomass is particularly interesting as a bulk modifier because it can introduce chemically heterogeneous and oxygen-containing domains into the graphite matrix without requiring highly engineered porous structures. Fruits native to the Brazilian Cerrado represent attractive biomass sources, including cagaita (*Eugenia dysenterica* DC). Previous characterization of *E. dysenterica* biomass revealed a composition rich in lignin and hemicellulose, providing a structurally consistent precursor containing

phenolic and oxygen-containing functionalities [8]. Mild torrefaction can partially transform this lignocellulosic matrix while avoiding the extensive processing associated with conventional high-temperature carbonization and chemical activation.

Despite the extensive literature on activated and carbonized biomass-derived electrode materials, it remains unclear whether a small fraction of mildly torrefied biomass incorporated directly into a conductive graphite matrix can significantly increase electrochemical accessibility without disrupting the conductive network. It is also important to determine whether any resulting enhancement arises predominantly from rapidly accessible surface regions or from slower charge-storage contributions associated with less readily accessible domains.

Therefore, this work investigates the direct incorporation of torrefied cagaita pulp biomass into a graphite–paraffin composite matrix as a low-processing strategy for modifying its charge-storage behavior. By systematically varying the biomass content, the study evaluates the balance between enhanced electrochemical accessibility and preservation of the conductive graphite framework, allowing identification of the composition that provides the optimum response. In addition to conventional capacitance measurements, scan-rate dependence, Trasatti analysis, galvanostatic charge–discharge, and chronoamperometric relaxation are used to examine how biomass incorporation modifies the relative contributions of rapidly and slowly accessible charge-storage regions. Rather than targeting highly engineered carbon materials for energy-storage devices, this proof-of-concept study uses capacitance as an electrochemical probe to determine whether a minimally processed

lignocellulosic material can substantially alter the interfacial behavior of a simple graphite–paraffin electrode.

2. Experimental

2.1. Preparation and characterization of torrefied biomass derived from cagaita (*Eugenia dysenterica*) pulp (TBCP)

Eugenia dysenterica DC fruits were collected in Sete Lagoas, Minas Gerais State, Brazil (19°28′36″ S, 44°11′43″ W) during 2024 and transported to the Chemistry Laboratory of the Federal University of São João del-Rei (UFSJ). The fruits were collected from native (wild) plants occurring in Cerrado areas of the UFSJ campus. The harvesting of Eugenia dysenterica DC fruits was conducted in accordance with Brazilian Law No. 12,727, dated October 17, 2012, which regulates the protection of native vegetation. Permission for plant collection was granted by the responsible institutional authority of UFSJ, as the collection was carried out on public land for non-commercial scientific research purposes, in compliance with Brazilian Law No. 12,651/2012 and Law No. 13,123/2015. Under these conditions, no specific governmental license was required for the collection of non-timber forest products. The plant species was taxonomically identified by Prof. Dr. Julio Onésio Ferreira Melo (Federal University of São João del-Rei, UFSJ), and a voucher specimen was deposited in the Herbário PAMG (Empresa de Pesquisa Agropecuária de Minas Gerais – EPAMIG), Belo Horizonte, Minas Gerais, Brazil, under voucher number PAMG 59803.

Cagaita pulp (1 kg) was milled in a knife mill for 20 min and subsequently subjected to torrefaction at 250 °C for 1 h under an air atmosphere. The

torrefaction temperature was selected based on the thermogravimetric profile of cagaita pulp and within the typical torrefaction range (200–300 °C), in which dehydration and partial decomposition of lignocellulosic components occur without extensive carbonization. The mild thermal treatment was intentionally employed to obtain a torrefied biomass while avoiding chemical activation or more energy-intensive carbonization procedures.

The resulting material was washed with distilled water until the conductivity of the washing water reached approximately 50 μS cm^{-1}. High-purity deionized water obtained from a Quimis deionization system was used throughout the experimental procedures. The resulting torrefied biomass derived from cagaita pulp was denoted as TBCP.

The surface functional groups of TBCP were characterized by Fourier-transform infrared spectroscopy with attenuated total reflection (FTIR/ATR), using an Agilent Cary 630 FTIR spectrophotometer (Agilent Technologies, USA).

Thermal analysis was performed at the Chemistry Department of the Federal University of Minas Gerais (UFMG) using Mettler thermal analysis equipment. Approximately 40 mg of the biomass sample was placed in an aluminum crucible and heated from 25 to 800 °C at a heating rate of 10 °C min^{-1} under synthetic air at a flow rate of 50 mL min^{-1}.

2.2. Preparation of graphite–paraffin/TBCP composite electrodes

Working electrodes were prepared using graphite powder, paraffin wax, and different amounts of torrefied biomass derived from cagaita pulp (TBCP). Initially, graphite powder (Merck 104206, density of 2.2 g cm^{-3} and average particle size of 120 μm) was mixed with TBCP to obtain powder mixtures

containing 0, 5, 10, and 15 wt% TBCP. The corresponding graphite content was adjusted accordingly to maintain a constant total powder mass.

Paraffin wax (0.075 g) was melted in a glass beaker on a hot plate at 80 °C for approximately 1 min. Subsequently, 0.425 g of the graphite/TBCP powder mixture was gradually added to the molten paraffin and mixed for 5 min at the same temperature to obtain a homogeneous composite. The total mass of each electrode batch was therefore maintained at 0.500 g.

The resulting composite was transferred to a cylindrical mold and compacted under a uniaxial load of 10 tons to form a self-supported cylindrical electrode. After compaction, the electrode was mounted in a polytetrafluoroethylene (PTFE) electrode holder equipped with an electrical contact, leaving only the circular electrode surface exposed to the electrolyte during electrochemical measurements. Prior to each electrochemical experiment, the exposed electrode surface was polished with 800-grit abrasive paper to obtain a reproducible surface.

TBCP was incorporated throughout the bulk graphite–paraffin matrix rather than deposited as a surface coating. Therefore, the TBCP content is expressed as the mass fraction incorporated into the graphite/TBCP powder mixture, and not as a conventional surface loading (mg cm^{-2}), since only an undefined fraction of the incorporated biomass is exposed at the electrochemically accessible electrode surface.

2.3. Electrochemical Characterization

Electrochemical measurements were performed in a conventional three-electrode cell using an Autolab potentiostat/galvanostat. The graphite–

paraffin/TBCP composite served as the working electrode (WE), a saturated Ag/AgCl electrode (KCl, sat.) was used as the reference electrode (RE), and a platinum wire was employed as the counter electrode (CE). Unless otherwise stated, all electrochemical measurements were carried out in 1.0 mol L^{-1} NaOH at room temperature.

The electrochemical behavior of the composite electrodes containing 0, 5, 10, and 15 wt% TBCP was initially evaluated by cyclic voltammetry (CV) over the potential range from −0.25 to +0.20 V vs. Ag/AgCl (KCl, sat.). The effect of TBCP incorporation on the capacitive response of the graphite–paraffin matrix was assessed by comparing the voltammetric profiles and the corresponding integrated charge. Cyclic voltammograms were recorded at different scan rates within the same potential window (ΔV = 0.45 V) to investigate the dependence of the charge-storage response on scan rate.

Chronopotentiometric measurements were performed under galvanostatic conditions using applied currents of 1×10^{-5}, 1×10^{-4}, and 1×10^{-3} A. Each current step was maintained for 5 s, and the resulting potential–time profiles were recorded to evaluate the charging and discharging behavior of the composite electrode under constant-current conditions.

Chronoamperometric measurements were also performed under potentiostatic conditions by alternately stepping the electrode potential between +0.20 and −0.25 V vs. Ag/AgCl (KCl, sat.). The resulting current–time transients were recorded to investigate the charging and discharging response of the electrode under potentiostatic conditions.

The capacitance obtained from cyclic voltammetry was calculated from the integrated voltammetric charge. When the integrated charge corresponded to a single voltammetric branch, the areal capacitance (C_A) was calculated according to Eq 1:

$$C_A = \frac{Q}{A\Delta V} \qquad (Eq.1)$$

where Q is the integrated charge, A is the geometric area of the electrode exposed to the electrolyte, and ΔV is the applied potential window (0.45 V). For chronopotentiometric measurements, the areal capacitance was determined from the discharge response according to Eq. 2:

$$C_A = \frac{I\Delta t}{A\Delta V} \qquad (\mathrm{Eq.}\,2)$$

where I is the applied current, Δt is the discharge time, and ΔV is the corresponding potential variation during discharge. A schematic overview of the complete experimental procedure is presented in Figure 1.

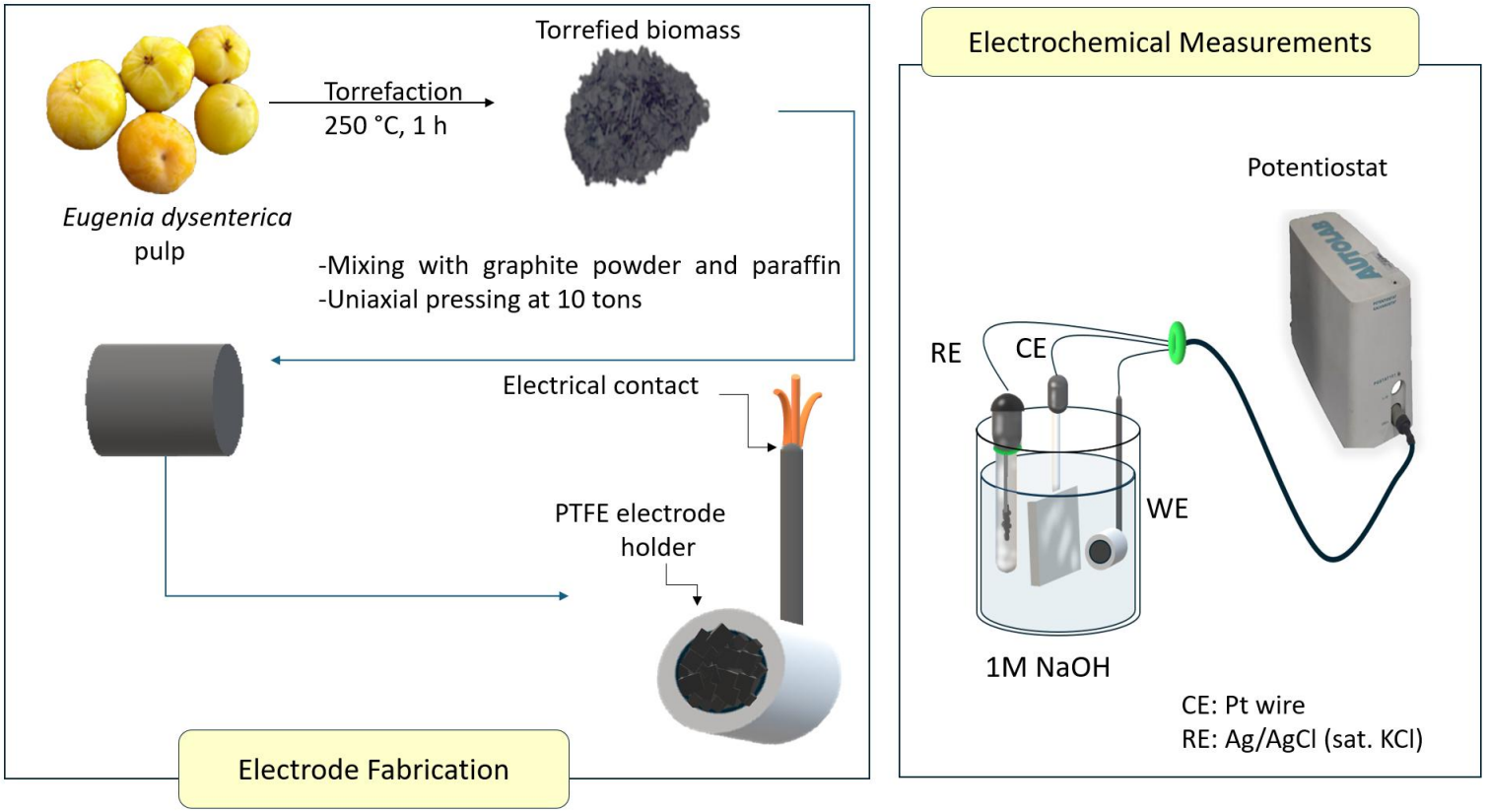


Figure 1. Schematic illustration of the preparation of graphite–paraffin/TBCP composite electrodes and the three-electrode electrochemical measurement setup in 1.0 mol L^{-1} NaOH.

3. Results

3.1. Thermogravimetric and Differential Thermal Analysis (TG/DTA) of Cagaita Pulp

Figure 2 shows the thermogravimetric (TG) and differential thermal analysis (DTA) curves of cagaita pulp. A pronounced endothermic event is observed at temperatures below approximately 100 °C and is attributed primarily to the removal of free and bound water, consistent with the high moisture content typically associated with fruit-derived biomass [9,11].

Between approximately 120 and 300 °C, the thermal behavior indicates progressive transformations of the lignocellulosic matrix, including the decomposition of low-molecular-weight constituents and the onset of hemicellulose degradation [11–13]. Hemicellulose is generally the lignocellulosic fraction most susceptible to thermal degradation within the torrefaction temperature range, whereas cellulose undergoes more extensive decomposition predominantly at higher temperatures [12,13].

The thermal behavior of cagaita pulp therefore supports the selection of 250 °C as the treatment temperature for TBCP production. This temperature lies within the range commonly employed for biomass torrefaction and promotes dehydration and partial degradation of the more thermally labile lignocellulosic constituents, particularly hemicellulose, while limiting the more extensive transformations associated with higher-temperature carbonization [12,13].

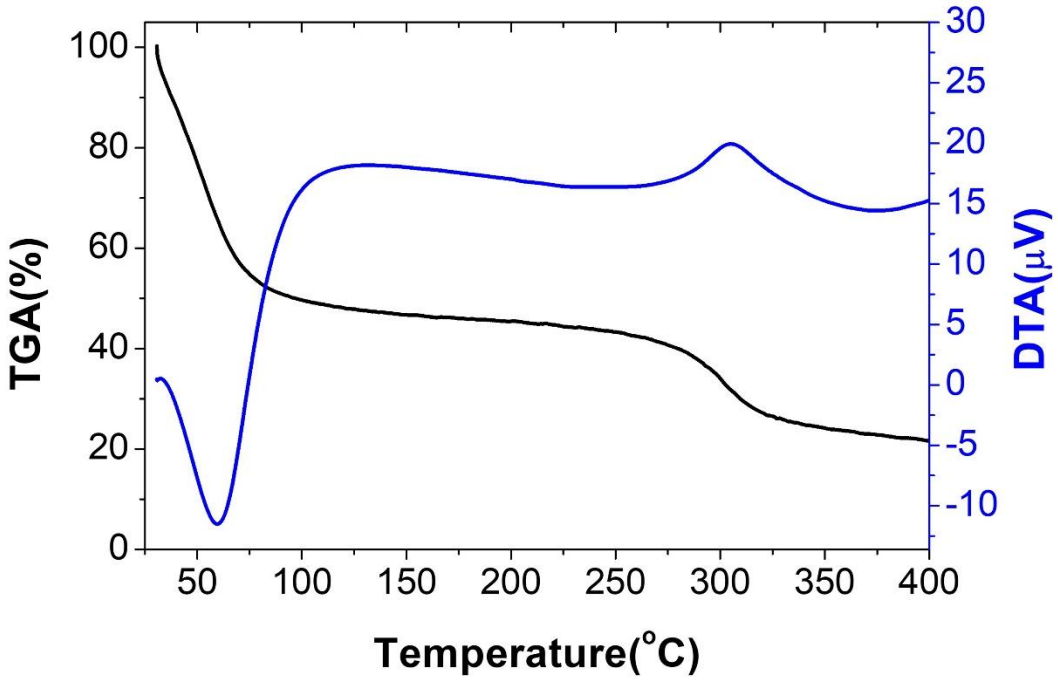


Figure 2. Thermogravimetric (TG) and differential thermal analysis (DTA) curves of cagaita pulp, highlighting the main dehydration and thermal decomposition regions.

3.2. FTIR analysis of cagaita pulp and TBCP

Figure 3 presents the FTIR spectra of raw cagaita pulp (CP) and torrefied biomass derived from cagaita pulp (TBCP), highlighting the chemical transformations induced by thermal treatment at 250 °C under air atmosphere.

The broad band centered at approximately 3314 cm^{-1} is assigned to O–H stretching vibrations of hydroxyl groups involved in hydrogen bonding, characteristic of cellulose, hemicellulose, lignin, and other oxygen-containing constituents of lignocellulosic biomass [12,13]. The marked attenuation of this band after thermal treatment is consistent with dehydration and changes in

hydroxyl-containing functionalities resulting from the thermal transformation of the lignocellulosic matrix during torrefaction.

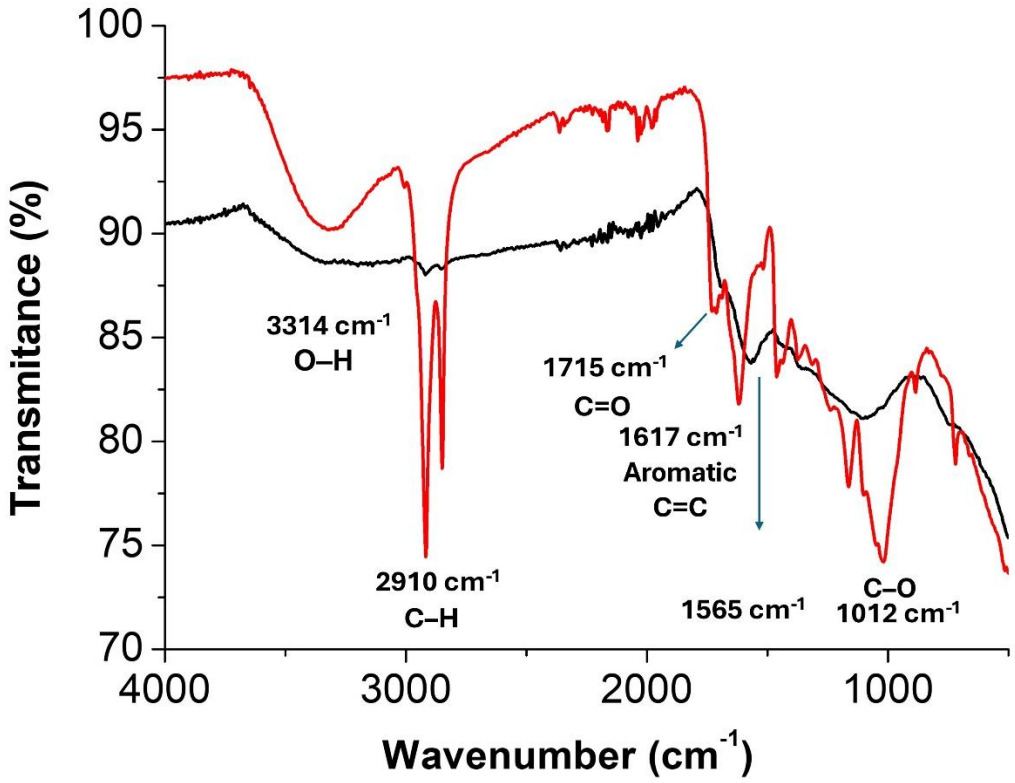


Figure 3. FTIR spectra of raw cagaita pulp (CP) and TBCP produced at 250 °C, highlighting the main spectral changes associated with thermal treatment, including the attenuation of hydroxyl-, aliphatic-, and oxygen-containing functionalities and structural changes in the lignocellulosic matrix.

The bands at approximately 2910 and 2835 cm^{-1} are assigned to asymmetric and symmetric C–H stretching vibrations of $–CH_2$ and $–CH_3$ groups, respectively. Their marked attenuation after thermal treatment indicates the loss of aliphatic structures and decomposition of thermally labile biomass constituents [12,13].

The band at approximately 1715 cm^{-1} is attributed to C=O stretching vibrations of carbonyl-containing functionalities. Its decreased intensity after treatment at 250 °C is consistent with transformations of oxygen-containing groups during torrefaction, including decarboxylation and deacetylation [12,13].

A notable change is also observed in the aromatic region, with the band shifting from approximately 1617 cm^{-1} in raw pulp to 1565 cm^{-1} in TBCP. This change is consistent with structural rearrangement of the lignocellulosic matrix and an increased contribution of aromatic structures [12,13]. In addition, attenuation of the band at approximately 1012 cm^{-1}, assigned mainly to C–O stretching of polysaccharide structures, is consistent with thermal modification and preferential degradation of hemicellulosic components [12-14].

Overall, the FTIR results indicate that treatment at 250 °C modifies the lignocellulosic structure of cagaita pulp while retaining oxygen-containing functionalities. These changes may influence electrode–electrolyte interactions when TBCP is incorporated into the graphite–paraffin matrix and may therefore contribute to its electrochemical behavior.

3.3. Electrochemical Characterization

A preliminary cyclic voltammetric scan over a wide potential range was performed to identify the electrochemical stability region of the system. As shown in Figure 4, pronounced cathodic and anodic currents develop at the negative and positive potential limits, respectively, indicating the onset of electrolyte decomposition. Therefore, a narrower potential window was selected for the subsequent capacitive measurements to minimize parasitic Faradaic reactions.

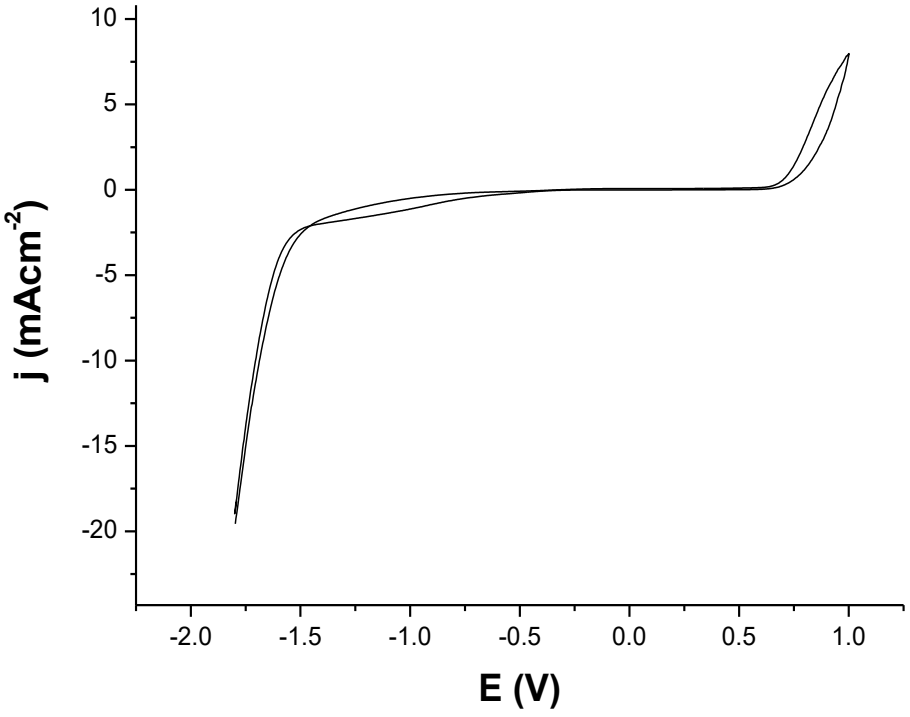


Figure 4. Cyclic voltammogram recorded over an extended potential range to evaluate the electrochemical stability region of the graphite–paraffin/TBCP electrode in 1.0 mol L^{-1} NaOH. The pronounced increase in current at the negative and positive potential limits indicates the onset of Faradaic processes.

Figure 5 compares the cyclic voltammograms recorded at 10 mV s^{-1} for the unmodified graphite–paraffin electrode (0 wt.% TBCP) and the electrode containing 5 wt.% TBCP. The incorporation of TBCP produces a pronounced increase in the voltammetric current and enclosed area, demonstrating the strong effect of the biomass-derived material on the charge-storage response of the graphite–paraffin matrix. For clarity, only the 0 and 5 wt.% electrodes are shown in Figure 5, since the substantially larger response of the 5 wt.% electrode makes

simultaneous visualization of all compositions difficult. The cyclic voltammograms of the remaining TBCP compositions, recorded under identical experimental conditions, are provided in the Supplementary Material (Figure S1).

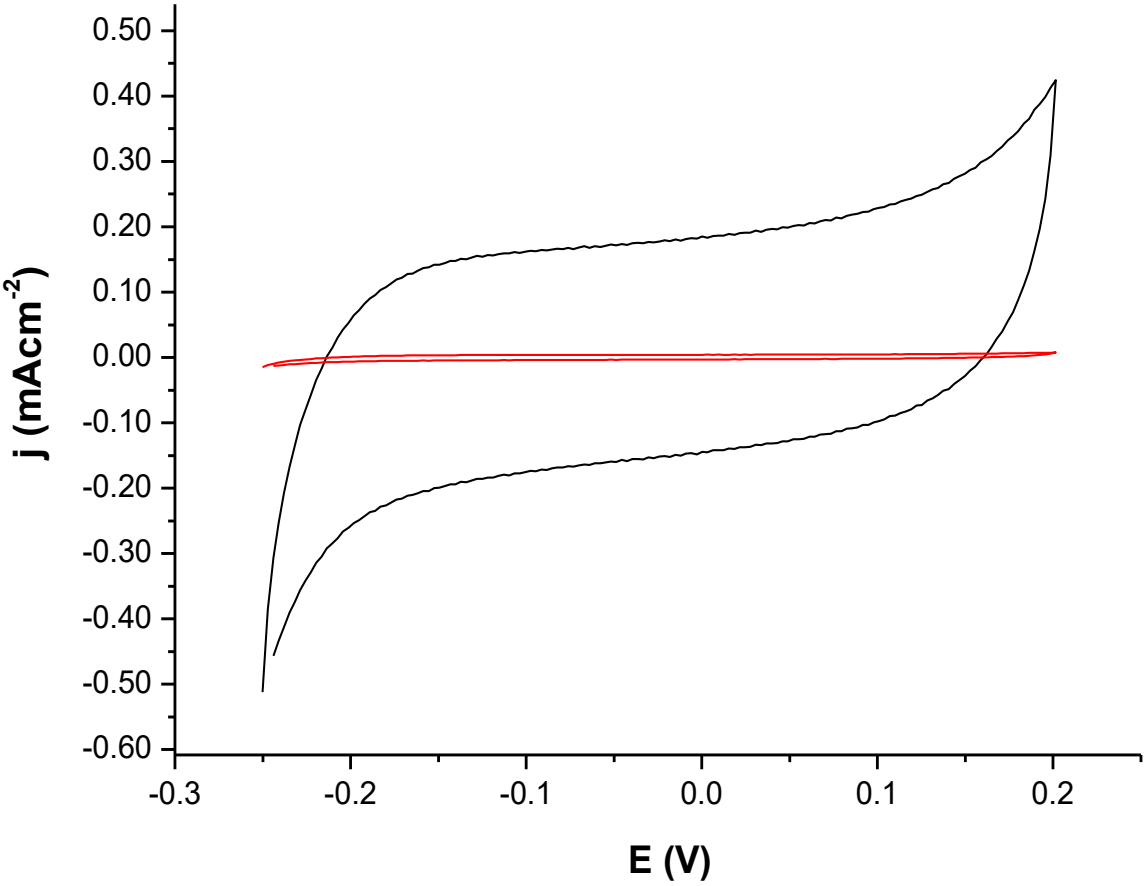


Figure 5. Cyclic voltammograms of graphite–paraffin electrodes containing 0 and 5 wt.% TBCP recorded at 10 mV s^{-1} in 1.0 mol L^{-1} NaOH.

The influence of TBCP content on the electrochemical response was subsequently evaluated by cyclic voltammetry within the selected potential window. The C_A was calculated from the integrated voltammetric charge according to Eq. (1). As shown in Figure 6, the incorporation of TBCP produced a strongly composition-dependent response. The areal capacitance increased

markedly upon TBCP addition, reaching a maximum of approximately 13 mF cm^{-2} at 5 wt.% TBCP. At higher TBCP contents, C_A decreased substantially. This non-monotonic behavior indicates that increasing the amount of biomass-derived carbon does not simply increase the electrochemically accessible charge-storage capacity. Instead, the maximum observed at 5 wt.% suggests an optimum balance between the additional electrochemically accessible surface introduced by TBCP and the preservation of an efficient conductive network provided predominantly by graphite. At higher TBCP contents, the progressive replacement of the more conductive graphite phase by the less conductive biomass-derived carbon may increasingly limit charge transport, offsetting the benefit associated with the additional surface.

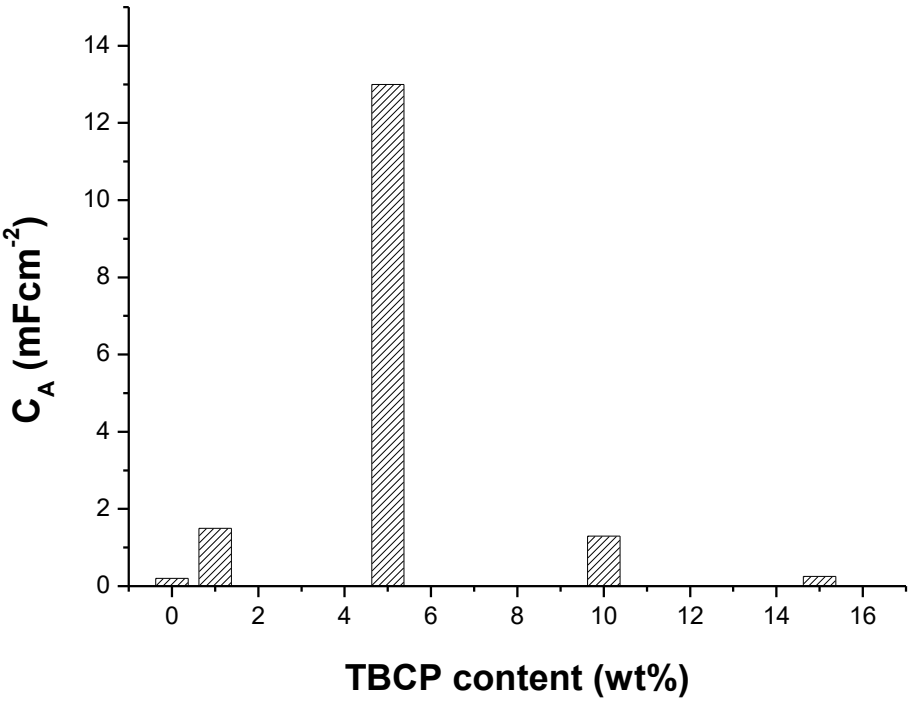


Figure 6. Areal capacitance (C_A) of graphite–paraffin composite electrodes as a function of TBCP content, calculated from cyclic voltammograms recorded at 10 mV s^{-1} in 1.0 mol L^{-1} NaOH.

Table 1 compares the present system with previously reported non-thin-film biomass-containing electrodes, including bulk, paste, thick, and three-dimensional electrode architectures. This comparison was selected because electrode geometry strongly influences ion accessibility, electrochemically active area, and areal capacitance, making thin-film and microsupercapacitor configurations less directly comparable with the compact graphite–paraffin/TBCP electrode investigated here.

The literature comparison also highlights substantial differences in processing intensity. El Hamdouni et al. [15] reported a graphite–paraffin paste electrode containing 15 wt% walnut-shell biochar produced at 600 °C under vacuum, which exhibited a C_{dl} of approximately 0.019 mF cm^{-2}. Zhang et al. [16] prepared 0.4-mm-thick biochar/PTFE electrodes from biomass carbonized at 500–700 °C under N_2, without chemical activation, obtaining areal C_{dl} values of approximately 0.016–3.11 mF cm^{-2}. Hammi et al. [17] reported a graphite–paraffin paste architecture particularly close to that employed in the present work, with C_{dl} values of 0.45–1.22 mF cm^{-2}; however, the biomass-derived carbon underwent hydrothermal carbonization, H_3PO_4 activation, thermal treatment at 550 °C under N_2, and subsequent TiO_2 incorporation. Similarly, Wang et al. [18] reported a three-dimensional bamboo-biochar electrode with a C_{dl} of 0.29 mF cm^{-2} for the unmodified biochar, whereas phosphorus doping and Pd/Cu incorporation increased C_{dl} to values as high as 7.74 mF cm^{-2}. In comparison, the present compact electrode reaches its maximum capacitive response with only 10 wt% TBCP obtained by thermal treatment at 300 °C in air, without chemical activation, inert-gas carbonization, metal loading, or additional surface functionalization. Thus, rather than competing with highly engineered porous

carbons, the present system demonstrates a favorable processing-to-performance balance, showing that significant capacitive enhancement can be achieved through a comparatively low-processing and low-biomass-loading strategy.

Table 1. Comparison of areal capacitance values reported for non-thin-film biomass-containing carbon electrodes.

Electrode composition	processing	Biomass loading	Capacitance	Determination method	Ref.
Graphite + 15 wt% biochar + paraffin oil; carbon-paste electrode	600 °C, 2 h, vacuum	15 wt%	0.019 mF cm^{-2}	EIS	[15]
Biochar + PTFE on stainless-steel mesh; 0.4-mm-thick electrode	500–700 °C, 2 h, N_2	Biochar major component	0.016–3.11 mF cm^{-2}*	EIS	[16]
Graphite + 20 wt% hydrochar/TiO_2 composite + paraffin oil; packed paste electrode	HTC 230 °C; H_3PO_4 activation; 550 °C/N_2; TiO_2 treatment	20 wt%	0.45–1.22 mF cm^{-2}	i_{cap}vs. scan rate	[17]
Biochar-based 3D particle electrode	Carbonization; modified samples additionally P-doped and metal-loaded	Biochar-based	0.29 mF cm^{-2} (BC); 1.19–7.74 mF cm^{-2} after modification	i_{cap}vs. scan rate	[18]
Graphite + paraffin + 10 wt% TBCP; compact bulk electrode	300 °C in air	10 wt%	≈4.5 mF cm^{-2}†	CV	This work

The effect of scan rate on the electrochemical response of the 5 wt.% TBCP electrode was further investigated by cyclic voltammetry. Figure 7 shows the voltammograms recorded at different scan rates within the selected potential window. As the scan rate increased, the current density increased systematically, while the overall shape of the voltammetric profiles was reasonably preserved. However, increasing distortion of the profiles was observed at higher scan rates, particularly near the potential limits. This behavior indicates that the charge-storage response is strongly dependent on the experimental timescale, suggesting that not all electrochemically accessible regions of the electrode can respond equally at high scan rates. At lower scan rates, the longer polarization time allows a larger fraction of the accessible surface and slower charge-storage processes to contribute to the measured response.

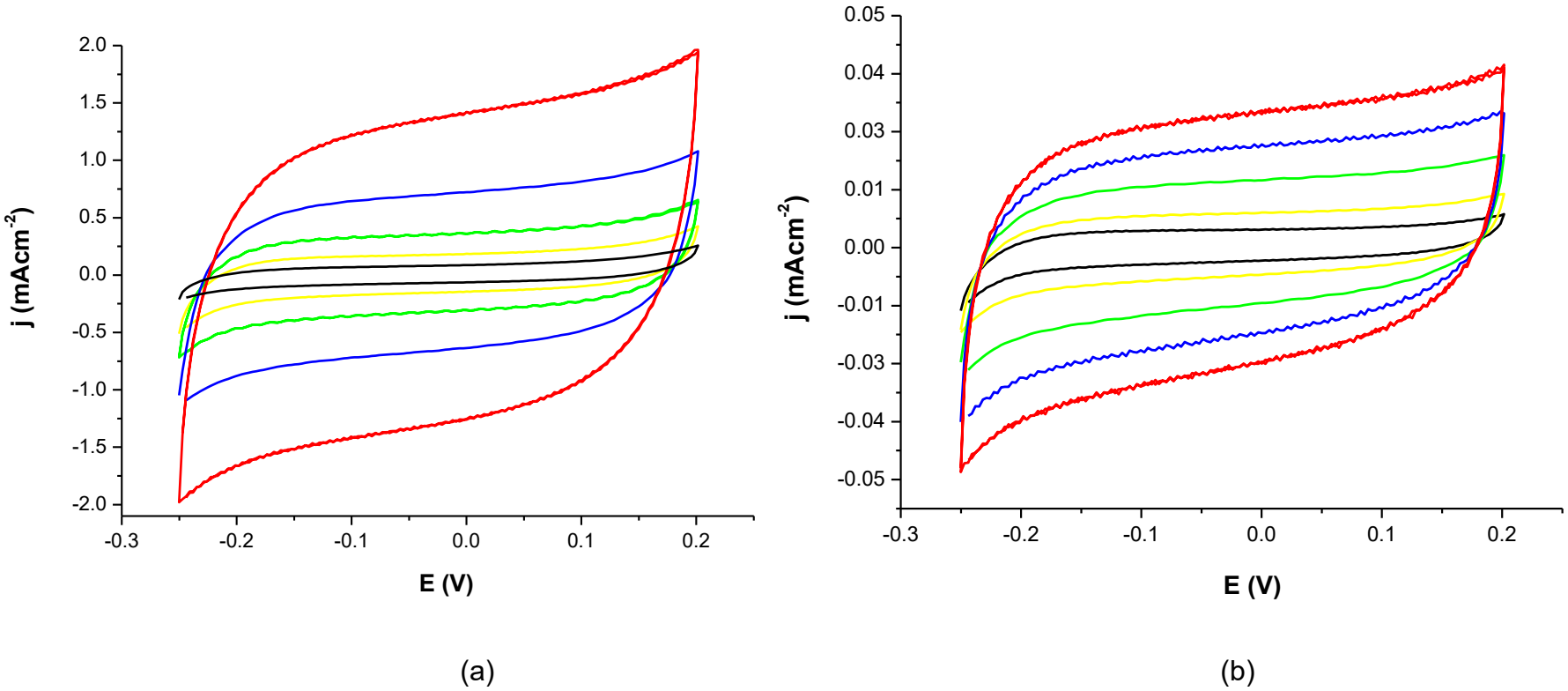


Figure 7. Cyclic voltammograms of the graphite–paraffin electrode containing 5 wt.% TBCP (a) and 0% wt.% TBCP recorded at different scan rates in 1.0 mol L^{-1} NaOH within the potential range from −0.25 to +0.20 V vs. Ag/AgCl.

To further investigate the rate-dependent accessibility of the charge-storage sites, the capacitance data were analyzed using the Trasatti method. In this approach, the relationship between areal capacitance and scan rate can be expressed as Eq.3, where C_{out} represents the capacitance associated with the readily accessible electrode surface and k_1 is a proportionality constant. Accordingly, extrapolation of C_A versus $v^{-1/2}$ to $v^{-1/2} = 0$ provides C_{out} (Figure 8a).

$$C_A = C_{\mathrm{out}} + k_1 v^{-1/2} \quad (Eq.3)$$

The total accessible capacitance can be estimated from the complementary Trasatti relationship (Eq. 4), where C_{total} corresponds to the limiting capacitance as $v \to 0$. Thus, extrapolation of $\frac{1}{C_A}$ versus $v^{1/2}$ to $v^{1/2} = 0$ yields $\frac{1}{C_{\mathrm{total}}}$ (Figure 8b). The contribution associated with less readily accessible regions can subsequently be estimated by $C_{\mathrm{in}} = C_{\mathrm{total}} - C_{\mathrm{out}}$. This analysis provides a useful estimate of the relative contributions of rapidly accessible and slower charge-storage regions to the overall electrochemical response.

$$\frac{1}{C_A} = \frac{1}{C_{\mathrm{total}}} + k_2 v^{1/2} \quad (Eq.4)$$

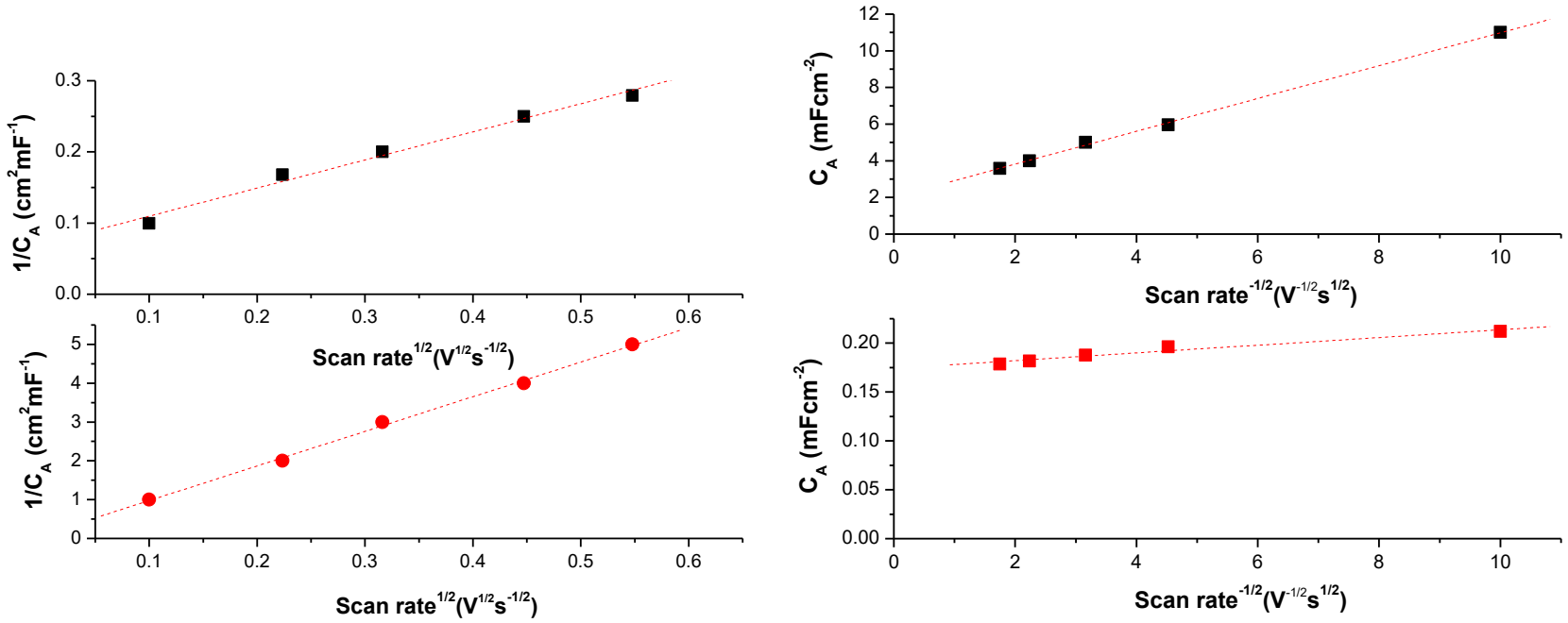


Figure 8. Trasatti plots for the electrodes containing 0 and 5 wt.% biomass. The linear extrapolations of $1/C_A$ versus $v^{1/2}$ and C_A versus $v^{-1/2}$ were used to estimate the outer (C_{out}) and total (C_{total}) capacitance contributions, respectively.

Based on these capacitance contributions, the apparent electrochemical porosity (P_{app}) can be estimated as the ratio between the less readily accessible capacitance and the total accessible capacitance:

$$P_{\mathrm{app}} = \frac{C_{\mathrm{in}}}{C_{\mathrm{total}}} \times 100 \qquad (Eq.5)$$

where C_{in} represents the capacitance associated with less readily accessible regions and C_{total} is the total accessible capacitance. This parameter provides an electrochemical estimate of the relative contribution of regions that become accessible at longer experimental timescales and should not be interpreted as the physical porosity determined by conventional textural characterization techniques. The capacitance contributions obtained from the Trasatti analysis, together with the corresponding apparent electrochemical porosity values, are summarized in Table 3.

Table 3. Capacitance parameters obtained from the Trasatti analysis for electrodes containing 0 and 5 wt.% biomass.

Parameter	**0 wt.%**	**5 wt.%**
C_{out} **(mF cm⁻²)**	0.178	2.22
C_{total}**(mF cm⁻²)**	0.219	25.68
C_{in} **(mF cm⁻²)**	0.041	23.46
Apparent porosity (%)	18.6	91.4

Figure 9 presents the charge–discharge chronopotentiograms obtained for the electrode containing 5% biomass at different applied currents. The capacitance was calculated from the slope of the potential–time profiles according to Eq 2. The variation in the charge–discharge time with the applied current reflects the current-dependent electrochemical response of the electrode.

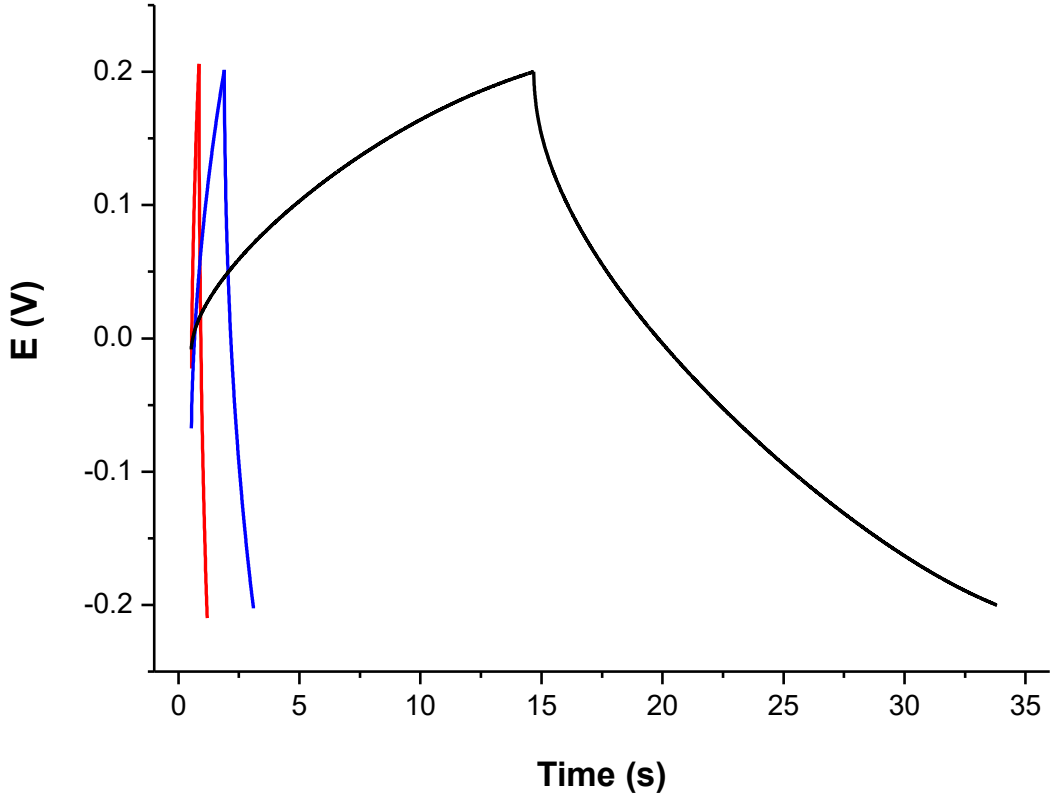


Figure 9. Galvanostatic charge–discharge chronopotentiograms of the electrode containing 5% biomass at different applied currents: 1.0×10^{-3} A (red), 5.0×10^{-4} A (blue) and $1x10^{-4}$A (black).

This current-dependent behavior is consistent with the results obtained from the Trasatti analysis. For the electrode containing 5% biomass, the total

capacitance was estimated as 25.68 mF cm^{-2}, of which 23.46 mF cm^{-2} was associated with the inner contribution, corresponding to an apparent porosity of 91.4%. Interestingly, the areal capacitance obtained at the lowest applied current (1.0×10^{-4} A) reached 21.05 mF cm^{-2}, corresponding to approximately 82% of the total capacitance estimated by the Trasatti method. This agreement suggests that lower currents provide sufficient time for ions to access electrochemically less accessible regions of the electrode. Conversely, at higher applied currents, only a smaller fraction of these sites can contribute effectively to charge storage because of kinetic and ion-transport limitations. Thus, the galvanostatic results are consistent with the high inner-capacitance contribution indicated by the Trasatti analysis. The areal capacitance values obtained at the different applied currents are summarized in Table 3.

Table 3. Electrochemical parameters obtained from the galvanostatic charge–discharge curves of the electrode containing 5% biomass at different applied currents.

I (A)	**C_A (mF cm^{-2})**
1.0×10^{-3}	4.02
5.0×10^{-4}	7.90
1.0×10^{-4}	21.05

3.4 Chronoamperometric transient analysis

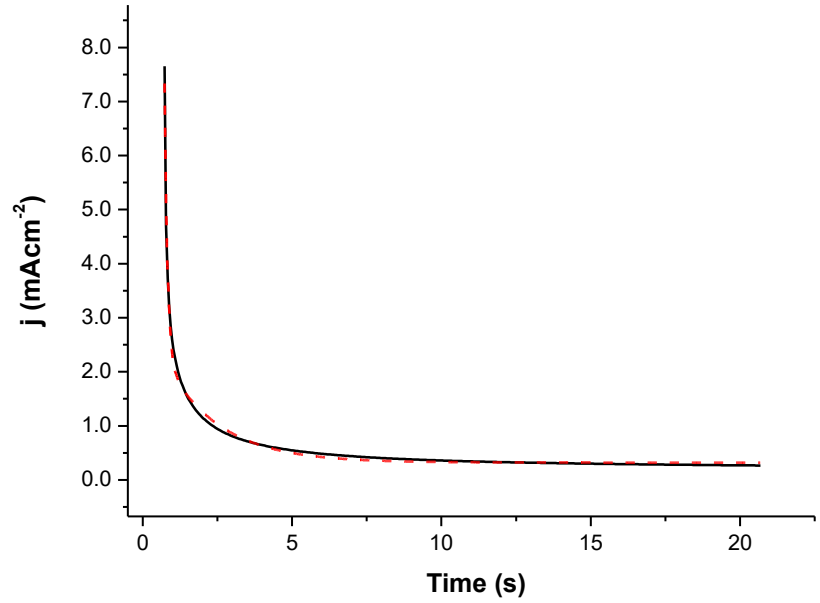
To further investigate the charge-storage dynamics of the electrodes containing 0 and 5 wt.% TBCP, the chronoamperometric transients recorded at 0.20 V, shown in Figures 10a and 10b, respectively, were analyzed using a biexponential decay function (Eq. 5) [19,20].

$$j(t) = j_{\infty} + A_1 \exp\left(-\frac{t}{\tau_1}\right) + A_2 \exp\left(-\frac{t}{\tau_2}\right) \quad (Eq.5)$$

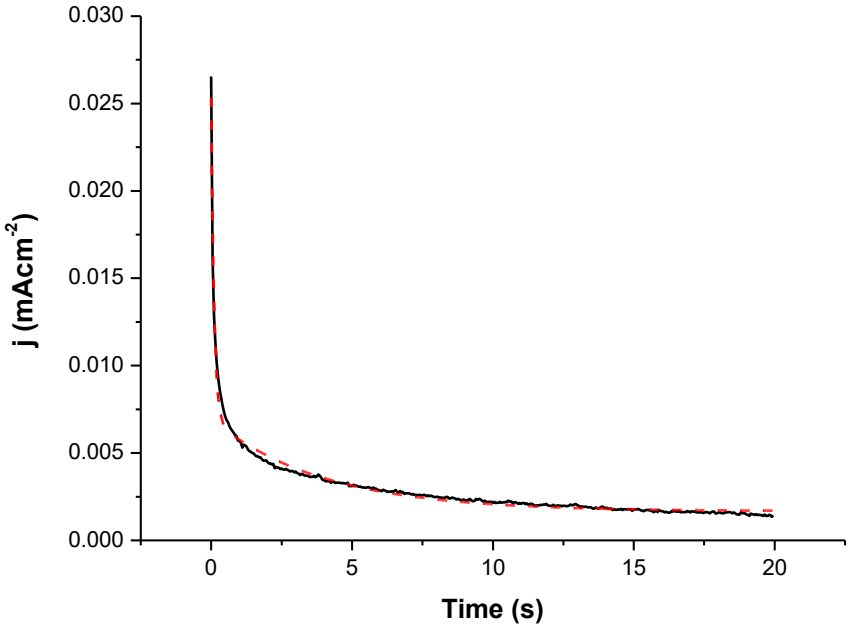
In Eq. 5, j_{∞} represents the residual current at long times, A_1 and A_2 are the amplitudes of the exponential components, and τ_1 and τ_2 are the corresponding characteristic relaxation times. The use of a multiexponential response is consistent with electrochemical systems containing more than one RC contribution, for which the current response to a potential step can be expressed as the sum of exponentially decaying terms. Moreover, Faradaic and non-Faradaic contributions may coexist in the transient response. The effective amplitude of each exponential component at the beginning of the experimentally recorded transient was calculated according to Eq. 6. The charge associated with each relaxation component was subsequently obtained by integration of the corresponding exponential term, resulting in Eq. 7. Finally, the apparent areal capacitance associated with each component was calculated according to Eq. 2.

$$A_{i,\mathrm{eff}} = A_i \exp\left(-\frac{t_0}{\tau_i}\right) \quad (Eq.6)$$

$$Q_i = A_{i,\mathrm{eff}}\tau_i \quad (Eq.7)$$



(a)



(b)

Figure 10. Chronoamperometric transient of the electrode containing 5 wt.% biomass recorded at an applied potential of 0.20 V. The dashed red line represents the biexponential fit used to determine the fast and slow relaxation components.

Accordingly, Table 4 summarizes the kinetic and charge-storage parameters obtained from the biexponential analysis of the 0 and 5 wt.% TBCP electrodes, including the characteristic relaxation times, effective amplitudes, charge contributions, and apparent areal capacitances associated with the fast and slow components. The total apparent areal capacitance was obtained from the sum of both contributions, allowing direct comparison of the charge-storage dynamics of the unmodified and biomass-containing electrodes.

Table 4. Parameters obtained from the biexponential analysis of the chronoamperometric transients of graphite–paraffin electrodes containing 0 and 5 wt.% TBCP at 0.20 V.

Parameter	**0 wt.% Fast**	**0 wt.% Slow**	**0 wt.% Total**	**5 wt.% Fast**	**5 wt.% Slow**	**5 wt.% Total**
τ (s)	0.1038 ± 0.0026	3.958 ± 0.100	—	0.0906 ± 0.0023	1.7439 ± 0.0353	—
$A_{i,\mathrm{eff}}$ (mA)	0.00679	0.00194	—	1.90	0.723	—
Q_i (mC)	0.000705	0.00769	0.00840	0.172	1.261	1.433
Relative charge contribution (%)	8.4	91.6	100	12.0	88.0	100
C_a (mF cm^{-2})	0.0095	0.104	0.113	2.33	17.04	19.37

The kinetic effect of TBCP incorporation becomes particularly relevant when the relative importance of the two relaxation components is considered. In both electrodes, the slow component accounts for most of the exponential charge (91.6% for 0 wt.% TBCP and 88.0% for 5 wt.% TBCP), whereas the fast contribution remains comparatively small. Therefore, the decrease in τ_{slow} from 3.958 to 1.744 s is more significant to the overall electrochemical response than the relatively small change in τ_{fast} from 0.1038 to 0.0906 s. This corresponds to an approximately 56% decrease in the characteristic slow relaxation time and a more than twofold increase in the corresponding relaxation rate ($1/\tau$). Notably, this faster relaxation of the dominant component is accompanied by a pronounced increase in its apparent areal capacitance, from 0.104 to 17.04 mF cm^{-2}. These results indicate that TBCP incorporation substantially increases the magnitude of the dominant charge-storage contribution while allowing it to relax on a shorter characteristic timescale.

This behavior may be related to the chemical and structural changes evidenced by FTIR. Torrefaction caused partial degradation of aliphatic and polysaccharide structures and increased the relative contribution of aromatic domains while retaining oxygen-containing functionalities. These remaining surface groups may favor electrode–electrolyte interactions and contribute to the substantially enhanced electrochemical response of the TBCP-containing composite.

4. Conclusion

The direct incorporation of torrefied cagaita pulp biomass into a graphite–paraffin matrix proved to be an effective low-processing strategy for modifying the charge-storage behavior of the electrode. Among the compositions investigated, 5 wt.% TBCP provided the highest electrochemical response, indicating an optimum balance between the additional electrochemically active contribution introduced by the biomass and preservation of the conductive graphite network. At higher TBCP contents, the decrease in capacitance suggests that progressive replacement of graphite increasingly limits charge transport.

The electrochemical analyses consistently demonstrated a pronounced enhancement of charge storage after TBCP incorporation. Trasatti analysis showed an increase in total accessible capacitance from 0.219 to 25.68 mF cm^{-2} and in apparent electrochemical porosity from 18.6 to 91.4%. Chronoamperometric analysis yielded a total apparent areal capacitance of 19.37 mF cm^{-2} for the 5 wt.% TBCP electrode, compared with only 0.113 mF cm^{-2} for the unmodified electrode. In both systems, the slow relaxation component accounted for most of the exponential charge; however, its characteristic time decreased from 3.958 to 1.744 s after TBCP incorporation, while its associated apparent capacitance increased markedly from 0.104 to 17.04 mF cm^{-2}. This indicates that TBCP not only increases the magnitude of the dominant charge-storage contribution, but also allows this contribution to relax on a shorter characteristic timescale. Galvanostatic measurements further supported the enhanced response, yielding 21.05 mF cm^{-2} at 1.0×10^{-4} A.

Together with the chemical modifications evidenced by FTIR, these results demonstrate that a small amount of mildly torrefied biomass can substantially alter the interfacial electrochemical behavior of graphite–paraffin electrodes without chemical activation, high-temperature carbonization, or complex electrode fabrication. The proposed strategy therefore provides a simple and sustainable route for enhancing charge storage in bulk carbon composite electrodes through minimal biomass processing.

DATA AVAILABILITY STATEMENT : The authors declare that the data supporting the findings of this study are available within the paper.

INTEREST STATEMENT : The authors declare that they have no conflict of interest

CLINICAL TRIAL REGISTRATION: Not applicable. This study does not involve a clinical trial.

FUNDING DECLARATION : The authors declare that they were not funded by any organization or fund.

AUTHOR CONTRIBUTIONS STATEMENT: E.M.G. conceived the study, performed the experiments, analyzed and interpreted the data, and wrote the manuscript. H.A.T., J.O.F.M., and A.P.C.M., contributed to the experimental work and data acquisition. All authors reviewed and approved the final manuscript.

CONSENT TO PUBLISH DECLARATION: Not applicable.

CONSENT TO PARTICIPATE DECLARATION: Not applicable.

ETHICS AND CONSENT TO PARTICIPATE: The plant material used in this study consisted of *Eugenia dysenterica* DC fruits collected from native plants in Cerrado areas of the Federal University of São João del-Rei (UFSJ) campus, Sete Lagoas, Minas Gerais, Brazil. The species was taxonomically identified by Prof. Dr. Julio Onésio Ferreira Melo (UFSJ), and a voucher specimen was deposited in the Herbário PAMG (Empresa de Pesquisa Agropecuária de Minas Gerais – EPAMIG), Belo Horizonte, Minas Gerais, Brazil, under voucher number PAMG 59803. Plant collection was conducted in accordance with applicable Brazilian legislation and institutional authorization.

REFERENCE

[1] Milne SA, Lasserre P, Corrigan DK. Fabrication of a graphite-paraffin carbon paste electrode and demonstration of its use in electrochemical detection strategies. *Analyst*. 2024;149(18):4736. DOI: 10.1039/D4AN00392F

[2] Oliveira JPPJ, Hiranobe CT, Torres GB, dos Santos RJ, Paim LL. Determination of Cr(VI) in leather residues using graphite/paraffin composite electrodes modified with reduced graphene oxide nanosheets. *Science of the Total Environment*. 2022;834:155318. DOI: 10.1016/j.scitotenv.2022.155318

[3] Gou G, Huang F, Jiang M, Li J, Zhou Z. Hierarchical porous carbon electrode materials for supercapacitor developed from wheat straw cellulosic foam. *Renewable Energy*. 2020;149:208. DOI: 10.1016/j.renene.2019.11.150.

[4] Treviño-Reséndez J, Soto-Hernández E, Godínez LA, Robles I, Meas Vong Y, García-Espinoza JD. Electrochemical oxidation of glyphosate using graphite rod electrodes: Impact of acetic acid pretreatment on degradation efficiency. *Processes*. 2024;12:2359. DOI: 10.3390/pr12112359.

[5] Los P, Lasia A, Fournier J, Brossard L, Ménard H. AC impedance studies of highly oriented pyrolytic graphite in 1M NaOH solution. *Journal of The Electrochemical Society*. 1994;141(10):2716. DOI: 10.1149/1.2059192.

[6] Iamprasertkun P, Hirunpinyopas W, Keerthi A, Wang B, Radha B, Bissett MA, Dryfe RAW. Capacitance of basal plane and edge-oriented highly ordered pyrolytic graphite: Specific ion effects. *The Journal of Physical Chemistry Letters*. 2019;10(4):617. DOI: 10.1021/acs.jpclett.8b03523.

[7] Pandolfo AG, Hollenkamp AF. Carbon properties and their role in supercapacitors. *Journal of Power Sources*. 2006;157(1):11. DOI: 10.1016/j.jpowsour.2006.02.065.

[8] Garcia EM, Taroco HA, Melo JOF. Highly efficient *Eugenia dysenterica* DC seeds biomass as adsorbent for methylene blue removal. *Discover Chemistry*. 2025;2:11. DOI: 10.1007/s44371-025-00086-2.

[9] Santos OV, Lorenzo ND, Souza ALG, Costa CEF, Conceição LRV, Lannes SCS, Teixeira-Costa BE. CO_2 supercritical fluid extraction of pulp and nut oils from *Terminalia catappa* fruits: Thermogravimetric behavior, spectroscopic and fatty acid profiles. *Food Research International*. 2021;139:109814. DOI: 10.1016/j.foodres.2020.109814.

[10] Chacón-Fernández MG, Hernández-Medel MR, Bernal-González M, Durán-Domínguez-de-Bazúa MC, Solís-Fuentes JA. Composition, properties, stability and thermal behavior of tamarind (*Tamarindus indica*) seed oil. *Grasas y Aceites*. 2019;70(4):e333. DOI: 10.3989/gya.0928182.

[11] Sharma A, Mohanty B. Thermal degradation of mango (*Mangifera indica*) wood sawdust in a nitrogen environment: Characterization, kinetics, reaction mechanism, and thermodynamic analysis. *RSC Advances*. 2021;11:13396. DOI: 10.1039/D1RA01467F.

[12] Ong HC, Yu KL, Chen W-H, Pillejera MK, Bi X, Tran KQ, Pétrissans A, Pétrissans M. Variation of lignocellulosic biomass structure from torrefaction: A critical review. *Renewable and Sustainable Energy Reviews*. 2021;152:111698. DOI: 10.1016/j.rser.2021.111698.

[13] Benavente V, Fullana A. Torrefaction of olive mill waste. *Biomass and Bioenergy*. 2015;73:186. DOI: 10.1016/j.biombioe.2014.12.020.

[14] Shen DK, Gu S, Bridgwater AV. The thermal performance of the polysaccharides extracted from hardwood: Cellulose and hemicellulose. *Carbohydrate Polymers*. 2010;82:39–45. DOI: 10.1016/j.carbpol.2010.04.018.

[15] El Hamdouni, Y.; El Hajjaji, S.; Szabó, T.; Trif, L.; Felhősi, I.; Abbi, K.; Labjar, N.; Harmouche, L.; Shaban, A. Biomass valorization of walnut shell into biochar as a resource for electrochemical simultaneous detection of heavy metal ions in water and soil samples: Preparation, characterization, and applications. *Arabian Journal of Chemistry* 2022, *15*, 104252. https://doi.org/10.1016/j.arabjc.2022.104252

[16] Zhang, Y.; Zhang, J.; Song, K.; Lv, W. Potential of biochar derived from three biomass wastes as an electrode catalyzing oxygen reduction reaction. *Environmental Pollutants and Bioavailability* 2022, *34*(1), 42–50. https://doi.org/10.1080/26395940.2021.2022538

[17] Hammi, Z.; Benhadria, E.H.; Lakhloufi, S.; Koumaiti, M.A.; Merbouh, L.; Labjar, N.; Lotfi, E.M.; Nasrellah, H.; Cherrat, A.; El Hajjaji, S. TiO_2-Doped Hydrochar Derived from *Phoenix dactylifera*: Synthesis and Electrocatalytic Performance for Alkaline Hydrogen Production. *Electrochem* 2026, *7*, 12. https://doi.org/10.3390/electrochem7020012

[18] Wang, D.; Zhang, L.; Dong, Y.; Wu, Y.; Zhu, Z.; Song, X.; Zhu, Y.; Liang, M. Enhanced N_2 production via 3D electrocatalytic nitrate reduction on Pd-Cu SACs by P-doped bamboo biochar. *iScience* 2026, *29*, 114428. https://doi.org/10.1016/j.isci.2025.114428

[19] Birbilis, N.; Nairn, K. M.; Forsyth, M. Transient response analysis of steel in concrete. *Corrosion Science* 2003, *45*, 1895–1902. https://doi.org/10.1016/S0010-938X(03)00086-6

[20] J.E. Ramón, A. Martínez-Ibernón, J.M. Gandía-Romero, R. Fraile, R. Bataller, M. Alcañiz, E. García-Breijo, J. Soto, Characterization of electrochemical systems using potential step voltammetry. Part I: Modeling by means of equivalent circuits, *Electrochim. Acta* 323 (2019) 134702. https://doi.org/10.1016/j.electacta.2019.134702